Energy-Efficient Fixed-Wing UAV Relay With Considerations of Airframe Shadowing

Daniel Bonilla Licea, *Member, IEEE*, Moises Bonilla E., Mounir Ghogho, *Fellow, IEEE*, and Martin Saska

***Abstract*— Owing to their high energy efficiency, fixed-wing unmanned aerial vehicles (UAVs) can operate as aerial relays to provide long periods of uninterrupted connectivity. In such systems, however, airframe shadowing may occur (i.e. the blockage of a UAV communication link by the UAV's own airframe) and can significantly degrade the communications performance. In this work, we propose a novel approach to optimize the trajectory of a fixed-wing UAV operating as a relay between a ground user (GU) and a ground base station (BS) to maximize the relay efficiency (defined as the ratio of the amount of relayed data to the consumed energy). We use the aerodynamic equations of the fixed-wing UAV to derive a semi-deterministic airframe shadowing model for loitering trajectories. Analytical expressions and simulation results illustrate the dependence of the airframe shadowing on the UAV's attitude and speed.**

***Index Terms*— Fixed-wing UAV, airframe shadowing, communications relay.**

I. Introduction

THE integration of UAVs into the communication network promises to enhance both its capacity and coverage [1], [2]. In this context, the use of UAVs as aerial communication relays has attracted significant interest [3], [4]. Various types of UAVs can be considered for this task, but the most common are: the multirotor UAV [5] and the fixed-wing UAV [6]. Unlike the fixed-wing UAV, the multirotor UAV can both take off and land vertically, as well as hover. But, the fixed-wing UAV is more energy efficient than the multirotor UAV in forward flight [7], [8]. Thus, fixed-wing UAVs can generally fly for longer durations, and are thus more suitable for applications where the aerial relay must uninterruptedly remain operational for long periods of time. But, since fixed-wing UAVs cannot hover above a ground target, they must loiter above it. When fixed-wing UAVs loiter around a target, they tilt (see Fig. 2(a)), causing their own airframe [9] to sometimes block their line of sight (LoS) with the ground nodes, thus degrading the signal-to-noise ratio (SNR). This is referred to as airframe shadowing and has been experimentally studied in the past [10], [11], [12], [13]. These experiments have confirmed that airframe shadowing can significantly degrade the communications performance. In [14], the authors experimentally derived a stochastic model of airframe shadowing and suggested that a deterministic model would be useful. But, as mentioned in recent surveys [15], [16], only a few papers have studied airframe shadowing and no deterministic models are available in the literature yet.

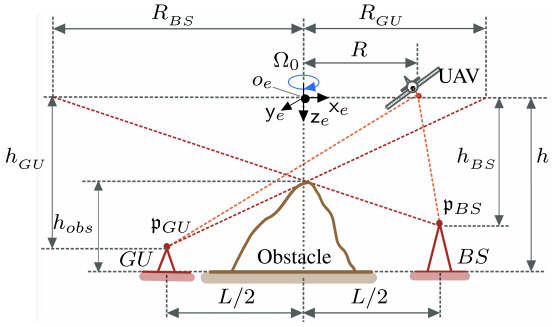

Fig. 1. Fixed-wing UAV acting as a relay between GU and BS.

Most of the literature dealing with UAVs for communications consider multirotor UAVs, but only a minority consider fixed-wing UAVs [8], [17]. In addition, the few papers dealing with fixed-wing UAVs for communications (e.g., [18], [19], and other references in [15] and [16]) do not consider airframe-shadowing, nor the dependency of the UAV attitude on its tangential speed and bank angle. This letter aims at filling this gap, we use the fixed-wing UAV aerodynamic equations on the stochastic airframe shadowing model in [14] to obtain a new airframe shadowing model suitable for communications-aware trajectory planning. Then, we use it to optimize the trajectory of a fixed-wing UAV, deployed at a fixed altitude h, acting as communications relay between a ground user (GU) and a base station (BS), see Fig. 1. A large obstacle impedes direct communication between the GU and the BS; communication is only possible via the UAV. We then optimize the UAV trajectory to maximize its efficiency (average relayed data over power consumed in flight), while considering the airframe shadowing. To the authors' best knowledge, this is the first time that airframe shadowing has been considered in a communications-aware trajectory planning for fixed-wing UAVs.

II. System Model

A. Fixed-Wing UAV

We denote the earth axes in which the UAV movement is described as $(o_e x_e y_e z_e)$ [20] (see Fig. 1). The horizontal plane $(o_e x_e y_e)$ is parallel to the earth surface and the $o_e z_e$ axis points

Manuscript received 4 March 2023; accepted 28 March 2023. Date of publication 5 April 2023; date of current version 12 June 2023. This work was partially funded by the European Union's Horizon 2020 research and innovation programme AERIAL-CORE under grant agreement no. 871479, by the Czech Science Foundation (GAC) under research project No. 20-10280S, and by OP VVV funded project CZ.02.1.01/0.0/0.0/16 019/0000765 "Research Center for Informatics". The associate editor coordinating the review of this letter and approving it for publication was Q. Wu. *(Corresponding author: Daniel Bonilla Licea.)*

Daniel Bonilla Licea and Martin Saska are with the Department of Cybernetics, Czech Technical University in Prague, 12135 Prague, Czech Republic (e-mail: bonildan@fel.cvut.cz; martin.saska@fel.cvut.cz).

Moises Bonilla E. is with CINVESTAV-IPN, Control Automático and Laboratorio, UMI, Mexico City 80060, Mexico (e-mail: mbonilla@cinvestav.mx).

Mounir Ghogho is with the TICLab, College of Engineering and Architecture, International University of Rabat, Rabat 11103, Morocco (e-mail: m.ghogho@ieee.org).

Digital Object Identifier 10.1109/LCOMM.2023.3264780

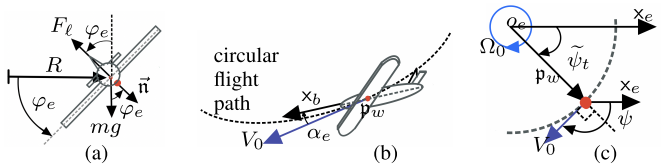

Fig. 2. Fixed-wing UAV; the UAV antenna is indicated by a red dot. (a) Front view; the UAV flies in a steady turn with a bank angle φ_e. (b) UAV lateral view; α_e is the angle of incidence. (c) Top view diagram.

vertically down along the gravity vector. Also, we define the body axes $(o_b \mathsf{x}_b \mathsf{y}_b \mathsf{z}_b)$ [20] placed on the lower UAV wing surface (see Fig. 2). The center o_b coincides with $\mathfrak{p}_w$; the axis z_b is aligned with the unitary normal wing vector $\vec{\mathfrak{n}}$; and the axes x_b and y_b lie along the wing center line and the lower center chord line, respectively (see Fig. 2(b)). The UAV flies with altitude h around $o_e \mathsf{z}_e$ in a circle of radius R, angular speed Ω_0, and constant angle of incidence α_e; $V_0 = \Omega_0 R$ is the tangential speed (see Fig. 1 and Fig. 2(b, c)). In the earth axes, the positions of the UAV, the BS, and the GU are:

$$\begin{aligned} \mathfrak{p}_w(\widetilde{\psi}_t) &= R \begin{bmatrix} \mathrm{c}(\widetilde{\psi}_t) & \mathrm{s}(\widetilde{\psi}_t) & 0 \end{bmatrix}^T, \\ \mathfrak{p}_{BS} &= \begin{bmatrix} \frac{L}{2} & 0 & h_{BS} \end{bmatrix}^T, \\ \mathfrak{p}_{GU} &= \begin{bmatrix} -\frac{L}{2} & 0 & h_{GU} \end{bmatrix}^T, \end{aligned} \tag{1}$$

where $\mathrm{c}(\cdot)$ and $\mathrm{s}(\cdot)$ are shorthand notations for $\cos(\cdot)$ and $\sin(\cdot)$; the BS and GU antennas heights are $h - h_{BS}$ and $h - h_{GU}$, see Fig. 1; L is the horizontal distance between the BS and the GU; $\widetilde{\psi}_t = \Omega_0 t$ is the UAV angular displacement in the circular trajectory of period $T = 2\pi/\Omega_0$. The UAV keeps constant the tangential speed V_0 and the bank angle φ_e, see Fig. 2(a). The trajectory radius R is related to the above variables as [20], [21]:

$$R = V_0^2/(g \tan\varphi_e), \quad \tan\varphi_e = V_0\,\Omega_0/g, \tag{2}$$

where g is the gravitational constant. The UAV lift force for small angles of incidence α_e can be expressed as:

$$F_\ell = \frac{1}{2} g\, V_0^2 S\, C_L, \quad C_L \approx C_{L_0} + C_{L_{\alpha_e}} \alpha_e, \tag{3}$$

where S is the wing area, C_L is the lift coefficient, and C_{L_0} is the camber lift coefficient. The linear lift coefficient force $C_{L_{\alpha_e}}$ can be approximated for small UAVs as $C_{L_{\alpha_e}} \approx \pi\,(b^2/S)/(1+\sqrt{1+(b^2/2S)^2})$ where b is the wingspan [21]. The lift force must compensate for the UAV's weight, i.e. $F_\ell \cos(\varphi_e) = m\,g$, where m is the UAV's mass (see Fig. 2(a)).

Let $\vec{\mathfrak{n}}$ denote the unitary normal wing vector, which is orthogonal to the bottom of the UAV wing surface and points downwards. In the earth axes coordinate frame, $\vec{\mathfrak{n}}$ is given by[1]:

$$\vec{\mathfrak{n}}\left(\widetilde{\psi}_t\right) \triangleq \begin{bmatrix} -\mathrm{c}(\varphi_e)\mathrm{s}(\alpha_e)\mathrm{s}(\widetilde{\psi}_t) + \mathrm{s}(\varphi_e)\mathrm{c}(\widetilde{\psi}_t) \\ \mathrm{c}(\varphi_e)\mathrm{s}(\alpha_e)\mathrm{c}(\widetilde{\psi}_t) + \mathrm{s}(\varphi_e)\mathrm{s}(\widetilde{\psi}_t) \\ \mathrm{c}(\varphi_e)\mathrm{c}(\alpha_e) \end{bmatrix}. \tag{4}$$

[1]For expressing the normal wing vector $\vec{n}$ in the earth axes, we need the *direction cosine matrix* D (see § 2.4 of [20]). The normal wing vector $\vec{n}$ expressed within the earth axes is: $\vec{\mathfrak{n}}\big|_e = D^{-1}\,\vec{\mathfrak{n}}\big|_b = D^T\,\vec{\mathfrak{n}}\big|_b$, where $\vec{\mathfrak{n}}\big|_b$ is the normal wing vector $\vec{n}$ expressed within the body axes, namely: $\vec{\mathfrak{n}}\big|_b = \begin{bmatrix} 0 & 0 & 1 \end{bmatrix}^T$. For our case, the Euler angles are (see Fig. 2): $(\phi,\, \theta,\, \psi) = \left(\varphi_e,\, \alpha_e,\, \pi/2 + \widetilde{\psi}_t\right)$. Thus, taking into account these angles in the *direction cosine matrix* D given by Eq. (2.12) of [20], and doing multiplications Equation (4) follows.

From [18], the power consumed by the fixed-wing UAV during of the circular trajectory can be expressed as:

$$P_t(V_0, R) = \left(c_1 + c_2/(gR)^2\right) V_0^3 + c_2/V_0, \tag{5}$$

the aerodynamic coefficients c_1 and c_2 come from the Drag coefficient given by $C_D = c_1 V_0^2 + c_2 (F_\ell/(mg)^2)/V_0^2$. Therefore, we have that $c_1 \triangleq \frac{1}{2}\rho\, C_{D_0} S$, and $c_2 \triangleq \frac{2(m\,g)^2}{\pi\, e_0\, b^2\, \rho}$, where C_{D_0} is the zero-lift drag coefficient and e_0 is the Oswald efficiency factor [18], [20], [21].

B. Communications System

The UAV has an antenna located at $\mathfrak{p}_w$ on its bottom wing surface (represented by a red dot in Fig. 2). To focus on the airframe shadowing, we assume that each ground node is equipped with a single isotropic antenna. The signal-to-noise ratio (SNR) of the GU-to-UAV and UAV-to-BS links can then be expressed as $\Gamma_i(t) = PG(\boldsymbol{\nu}_i) s_i(t) |a_i(t)|^2 / \left(\|\mathfrak{p}_i - \mathfrak{p}_w(\widetilde{\psi}_t)\|^2 \sigma^2\right)$, where $i = \{GU, BS\}$, σ^2 is the noise power at the receiver, P is the transmission power, $s_i(t)$ is the airframe shadowing term discussed in section III, $a_i(t)$ is the small-scale fading,[2] and $G(\boldsymbol{\nu}_i)$ is the power gain of three dimensional radiation pattern of the UAV antenna. Vectors $\boldsymbol{\nu}_{GU}$ and $\boldsymbol{\nu}_{BS}$ describe the angle of arrival (AoA) and angle of departure (AoD) (expressed in the UAV body frame) of the waves radiated from the GU to the UAV and from the UAV to the BS, respectively. Their components are the elevation and azimuth angles:

$$\boldsymbol{\nu}_i = \left[\mathrm{asin}\,(z_i)\,, \mathrm{asin}\left(x_i/\sqrt{x_i^2 + y_i^2}\right)\right], \tag{6}$$

$$[x_i, y_i, z_i] = \mathbf{D}^{\mathrm{T}}(\varphi_e, \alpha_e, \widetilde{\psi}_t) \left(\frac{\mathfrak{p}_i - \mathfrak{p}_w(\widetilde{\psi}_t)}{\|\mathfrak{p}_i - \mathfrak{p}_w(\widetilde{\psi}_t)\|}\right)^{\mathrm{T}}, \tag{7}$$

where $\mathbf{D}(\varphi_e, \alpha_e, \widetilde{\psi}_t)$ is the direction cosine matrix (see Eq. (2.12) of [20]). We assume frequency duplexing. The maximum bit rate achievable on each link is $r_{BS}(t) = B(1-\beta(t)) \log_2\left(1 + \Gamma_{BS}(t)\right)$ and $r_{GU}(t) = B\beta(t) \log_2\left(1 + \Gamma_{GU}(t)\right)$, where B is the total bandwidth available which is assumed to be small w.r.t. the carrier frequency, and the function $\beta(t) : \mathbb{R} \to [0, 1]$ controls the bandwidth distribution of both links. We equalize $r_{BS}(t)$ and $r_{GU}(t)$ by adjusting the value of $\beta(t)$. The maximum end-to-end bit rate becomes $r(t) = \frac{B \log_2(1+\Gamma_{BS}(t)) \log_2(1+\Gamma_{GU}(t))}{\log_2((1+\Gamma_{BS}(t))(1+\Gamma_{GU}(t)))}$.

III. Airframe Shadowing

In this section we first summarize the stochastic airframe shadowing model proposed in [14], then we modify it to generate a semi-deterministic airframe shadowing model suitable for communications-aware trajectory planning.

A. Stochastic Model [14]

Let $t^i_{j,s}$ mark the starting time of the jth airframe shadowing event between the UAV and the i node, and $D_{j,i}$ its duration.

[2]Without loss of generality we assume $\mathbb{E}[|a_i(t)|^2] = 1$.

Then, for $t \in [t^i_{j,s}, t^i_{j,s} + D_{j,i}]$, the shadowing loss due to the jth airframe shadowing (in dBs) event is:

$$L_{S_i}(t) = \underbrace{(A_0 + n(\varphi_e - \varphi_0) + X_{i,j})}_{\text{shadowing depth}} \underbrace{f\left((t - t^i_{j,s})/D_{j,i}\right)}_{\text{temporal variation}}, \tag{8}$$

where $L_{S_i}(t) \triangleq -10\log(s_i(t))$. The model is divided in two parts: the *shadowing depth* describes the shadowing severity, and the *temporal variation* describes its temporal evolution. In the *shadowing depth*, φ_0 is the minimum roll angle at which the model was fitted, A_0 is the airframe shadowing measured at φ_0, $n[\text{dB/rad}]$ is the rate at which the shadowing increases, and $X_{i,j}$ is a zero-mean Gaussian random variable which remains constant for the entire shadowing event. In the *temporal variation*, $f(t) : [0,1] \to [0,1]$ is a shape function that captures the gradual change of the airframe shadowing event observed experimentally, and it is a third order spline with four points of control: $f(0) = 0$, $f(1/2) = 1$, $f(0) = 0$, and $\frac{\mathrm{d}f(0)}{\mathrm{d}t} = 0$. Now, in [14], the airframe shadowing duration $D_{j,i}$ is modelled as a random variable, and there is no indication about how to determine the start of the airframe shadowing event $t^i_{j,s}$.

B. Semi-Deterministic Model

The stochastic model proposed in [14] and described in section III-B is not suitable to be used in communications-aware trajectory planning because the airframe shadowing duration is modelled as a random variable, and the model lacks a method to determine the start of an airframe shadowing event. But, as mentioned in [14], the airframe shadowing depends on the UAV flight manoeuvres, and these maneouvres are described by deterministic aerodynamic equations. Consequently, we use the aerodynamic equations of the fixed-wing UAV presented in section II-A to obtain a deterministic model for the occurrence and duration of the airframe shadowing. Then, we plug this deterministic description into the stochastic model (8) to obtain a semi-deterministic airframe shadowing model suitable for communications-aware trajectory planning.

To develop the airframe shadowing model, we first assume (as in [14]) that the UAV wing is the only airframe element that can obstruct the LoS between the UAV antenna and the ground nodes.[3] We abstract the wing as a flat linear plane of finite size. The carrier's wavelength must be significantly smaller than the size of the UAV wing so that airframe shadowing can occur. The aerodynamic UAV equations in section II-A determine the UAV attitude during the loitering trajectory. The UAV wing blocks the communications links when the transmission direction is on the opposite side of the bottom wing surface (see Fig. 1). This implies that the airframe shadowing occurs, on each communication link, when the following constraint is satisfied (see Figs. 1 and 2(c)):

$$\left(\mathfrak{p}_i - \mathfrak{p}_w(\widetilde{\psi}_t)\right)^T \vec{\mathfrak{n}}\left(\widetilde{\psi}_t\right) < 0, \tag{9}$$

[3]This is a simplification since the UAV tail could also block the LoS and/or the rest of the UAV airframe, but this effect is negligible in comparison with the wing shadowing in this antenna setup.

with $i = BS, GU$. Note that the l.h.s. of (9) is the inner product between the wing normal vector (4) (pointing towards the ground) and the vector pointing from the UAV antenna towards the ground nodes (BS or GU). When the (9) l.h.s. is positive, then the ground node sees the side of the wing where the antenna is mounted. When the l.h.s. of (9) is negative, the ground node sees the opposite side of the wing and does not see the antenna. For small values of the attack angle α_e, the l.h.s. of (9) can be approximated by the expression shown in Appendix A. Thus, we have:

$$\mathrm{c}\left(\widetilde{\psi}_t + \tilde{\Theta}_i\right) < \frac{R\mathrm{s}(\varphi_e) - h_i\mathrm{c}(\varphi_e) - \epsilon}{(L/2)\sqrt{\mathrm{s}^2(\varphi_e) + \alpha_e^2\mathrm{c}^2(\varphi_e)}}, \tag{10}$$

where $\tilde{\Theta}_i = \arctan\left(\frac{\alpha_e}{\tan(\varphi_e)}\right) + \Theta_i$ with $\Theta_{BS} = 0$ and $\Theta_{GU} = \pi$ (see Appendix A), and ϵ is the approximation error. If the r.h.s. in (10) is larger than 1 (smaller than -1), then (9) is always (never) satisfied, and thus the airframe shadowing is present (absent) during the full loitering trajectory. Because the approximation error ϵ is small, we can say that: 1) if (11a) is satisfied, it is likely that no airframe shadowing occurs; 2) if (11b) is satisfied, it is unlikely that any airframe shadowing occurs throughout the entire trajectory:

$$\frac{h_i\mathrm{c}(\varphi_e) - R\mathrm{s}(\varphi_e)}{(L/2)\sqrt{\mathrm{s}^2(\varphi_e) + \alpha_e^2\mathrm{c}^2(\varphi_e)}} \geq 1, \tag{11a}$$

$$\frac{R\mathrm{s}(\varphi_e) - h_i\mathrm{c}(\varphi_e)}{(L/2)\sqrt{\mathrm{s}^2(\varphi_e) + \alpha_e^2\mathrm{c}^2(\varphi_e)}} \geq 1. \tag{11b}$$

Finally, equation (9) jointly with the aerodynamic equations in section II-A provide a full deterministic description that indicates when an airframe shadowing occurs, and its duration. By merging this deterministic description with the stochastic model (8) we obtain a semi-deterministic model. This new semi-deterministic model is suitable for communication-aware trajectory planning for fixed-wing UAVs since it relates the airframe shadowing the UAV trajectory by means of (9).

IV. Problem Formulation

In this section, we show how to use our semideterministic airframe shadowing model presented in section III-B together with the aerodynamic equations of the fixed-wing UAV of section II-A in a communications-aware trajectory planning problem. Particularly, we consider the problem of optimizing the circular loitering trajectory of the fixed-wing aerial relay in Fig. 1 to maximize its efficiency.[4] The communication system is described in section II-B and the airframe shadowing model in section III-B. The variables controlled by the UAV, which remain constant during the whole trajectory, are its tangential speed V_0 and its bank angle φ_e. For the optimization, we replace the airframe shadowing loss (8) and the small-scale fading terms $|a_i(t)|^2$ with their expected values. The optimization problem is then formulated as follows:

$$\underset{\substack{V_0 \in [V_{min}, V_{max}] \\ \varphi_e \in [0, \varphi_{max})}}{\text{maximize}} \quad \frac{\frac{1}{T}\int_0^T \bar{r}(t)\mathrm{d}t}{\left(c_1 + \frac{c_2}{g^2\bar{R}^2}\right)V_0^3 + \frac{c_2}{V_0}} \tag{12}$$

[4]The ratio of the mean end-to-end data over the power spent in flying.

s.t.

$$\bar{r}(t) = \frac{Blog_2\left(1+\bar{\Gamma}_{BS}(t)\right)\log_2\left(1+\bar{\Gamma}_{GU}(t)\right)}{log_2\left(\left(1+\bar{\Gamma}_{BS}(t)\right)\left(1+\bar{\Gamma}_{GU}(t)\right)\right)}, \quad (13a)$$

$$\bar{\Gamma}_i(t) = PG(\boldsymbol{\nu}_i)\bar{s}_i(t)/\left(\|\mathfrak{p}_i - \mathfrak{p}_w(\widetilde{\psi}_t)\|^2\sigma^2\right), \quad (13b)$$

$$\bar{s}_i(t) = \mathbb{E}\left[10^{\frac{-L_{S_i}(t)}{10}}\right], \quad \alpha_e = \frac{2\,m/(V_0^2 Sc(\varphi_e)) - C_{L_0}}{C_{L_{\alpha_e}}}, \quad (13c)$$

$$R = V_0^2/(g\tan\varphi_e) \le R_{\max}, \quad \alpha_{\min} \le \alpha_e \le \alpha_{\max}, \quad (13d)$$

$$\mathfrak{p}_w(\widetilde{\psi}_t) = R\begin{bmatrix} c(\widetilde{\psi}_t) & s(\widetilde{\psi}_t) & 0\end{bmatrix}^{\mathrm{T}}, \quad \widetilde{\psi}_t = t\,V_0/R. \quad (13e)$$

where $T = 2\pi R/V_0$. The optimization target (12) is the ratio of the mean bit rate to the power spent in flying (see (5)). The expressions in (13a)-(13b) are obtained after replacing $|a_i(t)|^2$ with $\mathbb{E}[|a_i(t)|^2] = 1$ and the true airframe shadowing losses with their expected values, see $\bar{s}_i(t)$ in (13c). The SNRs (13b) depend on the AoA and AoD $\boldsymbol{\nu}_i$, which are calculated using (6)-(7). The tangential speed V_0 is constrained to be in $[V_{min}, V_{max}]$ where V_{min} is the minimum speed required for the UAV to keep flying and V_{max} depends on the maximum power of its motors. The bank angle φ_e is constrained to $[0, \varphi_{max})$ where $\varphi_{max} < \pi/4$ is imposed for safety reasons.

The incidence angle α_e is related to V_0 and φ_e by (13c) as derived from (3), and also due to $F_\ell\cos(\varphi_e) = m\,g$. Thus, the first term of (13d) relates the loitering trajectory radius R to V_0 and φ_e. The equality part of this first term is derived from (2), and ensures that the lift force always compensates for the UAV weight in order to keep the UAV flying. The inequality part of the first term limits the loitering UAV radius to $R_{max} = \min(R_{GU}, R_{BS})$ to avoid the obstacle mentioned previously from blocking the LoS between the UAV and the BS, see Fig. 1. Since the UAV is in the cruise flight phase [20], a minimum angle of incidence $\alpha_{min} > 0$ is needed. Then, to remain in the linear region of the *lift coefficient–angle of incidence curve*, C_L *vs.* α_e, we need $\alpha_e \le \alpha_{max}$. Otherwise, there can be a loss of lift force on the wing due to separation of the boundary layer. This is known as a stall [21], [22] and a control failure could occur as a result. These constraints are set on the second term of (13d). The loitering trajectory of the UAV is described by (13e). We can transform the constrained optimization problem (12)-(13e) to a simpler unconstrained optimization problem by incorporating the inequality constraints into the search space. The resulting equivalent and unconstrained optimization problem is:

$$\underset{\{V_0,\varphi_e\}\in\mathcal{X}}{\text{maximize}} \int_0^T \frac{\bar{r}(t)\mathrm{d}t}{T}\left(\left(c_1 + \frac{c_2}{g^2R^2}\right)V_0^3 + \frac{c_2}{V_0}\right)^{-1} \quad (14)$$

$$\text{s.t. } (13a)-(13c),\ (13e), \quad R = V_0^2/(g\tan\varphi_e), \quad (15)$$

with the search space

$$\mathcal{X} = \left\{\{V_0,\varphi_e\} : \varphi_e \in [0,\varphi_{max}), V_0 \in [\underline{V}(\varphi_e), \overline{V}(\varphi_e)]\right\}$$

$$\underline{V}(\varphi_e) = \max\left(V_{min}, V_{\alpha_{max}}(\varphi_e)\right)$$

$$\overline{V}(\varphi_e) = \min\left(V_{max}, V_{\alpha_{min}}(\varphi_e), \sqrt{R_{max}g\tan(\varphi_e)}\right)$$

$$V_\alpha(\varphi_e) = \sqrt{2m/\left((C_{L_{\alpha_e}}\alpha + C_{L_0})Sc(\varphi_e)\right)} \quad (16)$$

In general, the optimization target (14) has multiple local maxima. But the search space $\mathcal{X}$ is bounded, then (14)-(16) can be solved numerically by establishing a fine grid over $\mathcal{X}$, and then solve it with simulated annealing [23] or any other optimization algorithm that can deal with multiple maxima.

V. Simulations

We consider the fixed-wing UAV called Aerosonde whose aerodynamic coefficients are given in Table E.2, Appendix E of [21], namely: $m = 13.5$ [kg], $S = 0.55$ [m^2], $b = 2.8956$ [m], $\rho = 1.2682$ [kg/m^3], $e_0 = 0.9$, $C_{L_0} = 0.28$, $C_{D_0} = 0.03$, and $C_{L_\alpha} = 3.45$. We choose $P/\sigma^2 = 10^5$, $L = 300$[m], $h - h_{BS} = 10$[m], $h - h_{GU} = 1$[m], $h = 60$[m], $V_{min} = 10$[m/s], $V_{max} = 20$[m/s], $\varphi_{max} = \pi/4$[rad], $\alpha_{min} = \pi/180$[rad], $\alpha_{max} = \pi/18$[rad], $R_{max} = 300$[m]. We then use the same airframe shadowing parameters values given in [14] for the communications in band C. We consider the antenna radiation power pattern used in [24], which represents an antenna with moderate directivity. We then compare two UAV trajectories. The first trajectory, used as a benchmark, is obtained by solving (12)-(13c), while disregarding the airframe shadowing (i.e., we set $L_{S_i}(t) = 0$ for $i = \{BS, GU\}$ and for all t in the optimization). This benchmark trajectory has the following characteristics: tangential speed $V_0 = 10$[m/s], bank angle $\varphi_e = 45$[°], angle of attack $\alpha_e = 6.8797$[°], loitering radius $R = 10.1937$[m], and trajectory period $T = 6.4049$[s]. The second trajectory is obtained by solving (12)-(13c) with our semideterministic airframe shadowing model presented in section (III-B). This *Airframe Shadowing Aware* (ASA) trajectory has the following characteristics: tangential speed $V_0 = 10$[m/s], bank angle $\varphi_e = 12.2034$[°], angle of attack $\alpha_e = 3.6078$[°], loitering radius $R = 63.2700$[m], and trajectory period $T = 39.7537$[s].

In the benchmark trajectory, the UAV *tries to remain atop* the middle ground point between the GU and the BS. It achieves this by setting a large bank angle φ_e that produces a small loitering radius R. But, this large bank angle causes airframe shadowing in both communication links, see Fig. 3. At its worst, the airframe shadowing introduces almost 20 dBs of loss. In the ASA trajectory, the bank angle φ_e is small, and the inequality (11a) is satisfied for both links. As mentioned in section III-B, this implies that no airframe shadowing appears. This is confirmed by the simulation results where the UAV antenna maintains LoS at all times with the BS and with the GU. Thus, the ASA trajectory is free of airframe shadowing.

When we compare the ASA trajectory w.r.t. the benchmark trajectory (see Fig. 3) we observe that it has a peak end-to-end bit rate 46.15% larger, an average end-to-end bit rate 157.79% larger, a power consumption 19.52% lower, and a total efficiency 220.33% larger. Furthermore, the minimum instantaneous bit rate obtained with the ASA trajectory is also greater. In summary, by taking into account the airframe shadowing in the optimization, the fixed-wing UAV can achieve a greater average bit rate while reducing its energy consumption, resulting in a greater efficiency.

Finally, to complete the analysis we compare the fixed-wing UAV ASA trajectory w.r.t. to a multirotor UAV of the same

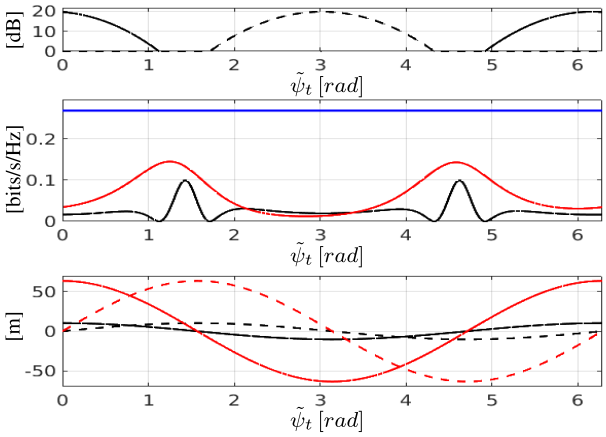

Fig. 3. Top: airframe shadowing loss of each link for the benchmark trajectory; $L_{S_{GU}}$ (continuous line) and $L_{S_{BS}}$ (dashed line). Middle: normalized end-to-end bit rate $r(\widetilde{\psi}_t)/B$ for the benchmark trajectory (black), the ASA trajectory (red), and the multirotor UAV (blue). Bottom: benchmark trajectory (black), and ASA trajectory (red); x components in continuous lines, and y components in dashed lines.

mass m operating as a relay located in the center of the fixed-wing UAV loitering trajectory. The fixed-wing UAV obtains an average bit rate 75.89% lower, but consumes 89.18% less power,[5] and thus is 143.16% more efficient.

VI. Conclusion

A novel approach to optimize the loitering trajectory of a fixed-wing UAV relay considering airframe shadowing and energy consumption during its flight was presented in this letter. We proposed a semi-deterministic airframe shadowing model that builds on an experimentally validated stochastic model and uses the fixed-wing UAV aerodynamic equations. Analytical derivations and simulations have shown that the airframe shadowing profile depends on the bank angle φ_e and on the angle of incidence α_e, which further depends on the UAV tangential speed. Simulation results demonstrate that taking the airframe shadowing into account during optimization leads to an increased performance of the UAV. Future work will attempt to develop a more comprehensive deterministic airframe shadowing model that can be used in more general scenarios for trajectory planning purposes.

Appendix

A. Phase Displacement

When the incidence angle α_e is small, we acquire the following from (1) and (4) $\left(\mathfrak{p}_i - \mathfrak{p}_w\left(\widetilde{\psi}_t\right)\right)^T \vec{\mathfrak{n}}\left(\widetilde{\psi}_t\right) \approx k_1 \mathrm{c}\left(\widetilde{\psi}_t + \chi + \Theta_i\right) + k_2$, where $i = \{BS, GU\}$, $k_1 = (L/2)\sqrt{\mathrm{s}^2(\varphi_e) + \alpha_e^2 \mathrm{c}^2(\varphi_e)}$, $\chi = \arctan(\alpha_e / \tan(\varphi_e))$, $\Theta_{BS} = 0$, $\Theta_{GU} = \pi$, and $k_2 = h_i \mathrm{c}(\varphi_e) - R\,\mathrm{s}(\varphi_e)$.

References

[1] Y. Zeng, Q. Wu, and R. Zhang, "Accessing from the sky: A tutorial on UAV communications for 5G and beyond," *Proc. IEEE*, vol. 107, no. 12, pp. 2327–2375, Dec. 2019.

[5]For the power consumption of the multirotor UAV we use the formula experimentally derived in [25].

[2] D. Mishra and E. Natalizio, "A survey on cellular-connected UAVs: Design challenges, enabling 5G/B5G innovations, and experimental advancements," *Comput. Netw.*, vol. 182, Dec. 2020, Art. no. 107451.
[3] M. T. Dabiri and S. M. S. Sadough, "Optimal placement of UAV-assisted free-space optical communication systems with DF relaying," *IEEE Commun. Lett.*, vol. 24, no. 1, pp. 155–158, Jan. 2020.
[4] D. B. Licea, G. Silano, M. Ghogho, and M. Saska, "Optimum trajectory planning for multi-rotor UAV relays with tilt and antenna orientation variations," in *Proc. 29th Eur. Signal Process. Conf. (EUSIPCO)*, Aug. 2021, pp. 1586–1590.
[5] D. B. Licea, M. Bonilla, M. Ghogho, S. Lasaulce, and V. S. Varma, "Communication-aware energy efficient trajectory planning with limited channel knowledge," *IEEE Trans. Robot.*, vol. 36, no. 2, pp. 431–442, Apr. 2020.
[6] P. Poksawat, L. Wang, and A. Mohamed, "Gain scheduled attitude control of fixed-wing UAV with automatic controller tuning," *IEEE Trans. Control Syst. Technol.*, vol. 26, no. 4, pp. 1192–1203, Jul. 2018.
[7] K. Karydis and V. Kumar, "Energetics in robotic flight at small scales," *Interface Focus*, vol. 7, no. 1, Feb. 2017, Art. no. 20160088.
[8] Q. Wu et al., "A comprehensive overview on 5G-and-beyond networks with UAVs: From communications to sensing and intelligence," *IEEE J. Sel. Areas Commun.*, vol. 39, no. 10, pp. 2912–2945, Oct. 2021.
[9] R. F. Stengel, *Flight Dynamics*. Princeton, NJ, USA: Princeton Univ. Press, 2004.
[10] R. Sun and D. W. Matolak, "Initial results for airframe shadowing in L- and C-band air-ground channels," in *Proc. Integr. Commun., Navigat. Surveill. Conf. (ICNS)*, Apr. 2015, pp. X1-1–X1-8.
[11] D. W. Matolak, R. Sun, H. Jamal, and W. Rayess, "L- and C-band airframe shadowing measurements and statistics for a medium-sized aircraft," in *Proc. 11th Eur. Conf. Antennas Propag. (EUCAP)*, Mar. 2017, pp. 1429–1433.
[12] Y. S. Meng and Y. H. Lee, "Study of shadowing effect by aircraft maneuvering for air-to-ground communication," *AEU-Int. J. Electron. Commun.*, vol. 66, no. 1, pp. 7–11, 2012.
[13] J. Kunisch et al., "Wideband time-variant air-to-ground radio channel measurements at 5 GHz," in *Proc. Eur. Conf. Antennas Propag. (EUCAP)*, 2011, pp. 1386–1390.
[14] R. Sun, D. W. Matolak, and W. Rayess, "Air-ground channel characterization for unmanned aircraft systems—Part IV: Airframe shadowing," *IEEE Trans. Veh. Technol.*, vol. 66, no. 9, pp. 7643–7652, Sep. 2017.
[15] A. A. Khuwaja, Y. Chen, N. Zhao, M.-S. Alouini, and P. Dobbins, "A survey of channel modeling for UAV communications," *IEEE Commun. Surveys Tuts.*, vol. 20, no. 4, pp. 2804–2821, 4th Quart., 2018.
[16] W. Khawaja, I. Guvenc, D. W. Matolak, U.-C. Fiebig, and N. Schneckenburger, "A survey of air-to-ground propagation channel modeling for unmanned aerial vehicles," *IEEE Commun. Surveys Tuts.*, vol. 21, no. 3, pp. 2361–2391, 3rd Quart., 2019.
[17] B. Li, Z. Fei, and Y. Zhang, "UAV communications for 5G and beyond: Recent advances and future trends," *IEEE Internet Things J.*, vol. 6, no. 2, pp. 2241–2263, Apr. 2019.
[18] Y. Zeng and R. Zhang, "Energy-efficient UAV communication with trajectory optimization," *IEEE Trans. Wireless Commun.*, vol. 16, no. 6, pp. 3747–3760, Jun. 2016.
[19] J. Ouyang, Y. Che, J. Xu, and K. Wu, "Throughput maximization for laser-powered UAV wireless communication systems," in *Proc. IEEE Int. Conf. Commun. Workshops (ICC Workshops)*, May 2018, pp. 1–6.
[20] M. Cook, *Flight Dynamics Principles: A Linear Systems Approach to Aircraft Stability and Control*, 3rd ed. Amsterdam, The Netherlands: Elsevier, 2013.
[21] R. W. Beard and T. W. McLain, *Small Unmanned Aircraft: Theory and Practice*. Princeton, NJ, USA: Princeton Univ. Press, 2012.
[22] T. Faure *Dinamique Des Fluides Appliquée, Applications a L'aerodynamique*. Paris, France: Dunod, 2008.
[23] D. Bertsimas and J. Tsitsiklis, "Simulated annealing," *Statist. Sci.*, vol. 8, no. 1, pp. 10–15, 1993.
[24] D. B. Licea, E. Nurellari, and M. Ghogho, "Energy-efficient 3D UAV trajectory design for data collection in wireless sensor networks," in *Proc. IEEE Int. Conf. Acoust., Speech Signal Process. (ICASSP)*, May 2020, pp. 8329–8333.
[25] Z. Liu, R. Sengupta, and A. Kurzhanskiy, "A power consumption model for multi-rotor small unmanned aircraft systems," in *Proc. Int. Conf. Unmanned Aircr. Syst. (ICUAS)*, Jun. 2017, pp. 310–315.